The Role of Rare-Earth Atoms in the Anisotropy and Antiferromagnetic Exchange Coupling at a Hybrid Metal–Organic Interface

María Blanco-Rey,* Rodrigo Castrillo, Khadiza Ali, Pierluigi Gargiani, Maxim Ilyn, Michele Gastaldo, Markos Paradinas, Miguel A. Valbuena, Aitor Mugarza, J. Enrique Ortega, Frederik Schiller, and Laura Fernández*

Magnetic anisotropy and magnetic exchange interactions are crucial parameters that characterize the hybrid metal–organic interface, a key component of an organic spintronic device. It is shown that the incorporation of $4f$ RE atoms to hybrid metal–organic interfaces of CuPc/REAu$_2$ type (RE = Gd, Ho) constitutes a feasible approach toward on-demand magnetic properties and functionalities. The GdAu$_2$ and HoAu$_2$ substrates differ in their magnetic anisotropy behavior. Remarkably, the HoAu$_2$ surface promotes the inherent out-of-plane anisotropy of CuPc, owing to the match between the anisotropy axis of substrate and molecule. Furthermore, the presence of RE atoms leads to a spontaneous antiferromagnetic exchange coupling at the interface, induced by the $3d$–$4f$ superexchange interaction between the unpaired $3d$ electron of CuPc and the $4f$ electrons of the RE atoms. It is shown that $4f$ RE atoms with unquenched quantum orbital momentum (L), as it is the case of Ho, induce an anisotropic interfacial exchange coupling.

1. Introduction

Molecular spintronics is an emerging field that combines ferromagnetic materials with organic or metal–organic semiconductors. It benefits from the unique and exceptional properties of organic molecules, which go beyond inorganics.[1–6] Furthermore, the strong response of many organic molecules to electrical, optical or magnetic stimuli bring new potential functionalities to the spintronic device.[7–12] An effective spin tunneling between the ferromagnet and the organic molecule is governed by the so-called spinterface that is formed by the hybrid interface between both materials. The spinterface is defined on the one hand by the energy level alignment between molecule and ferromagnet, and on the other hand by its anisotropy and the interfacial magnetic exchange interaction.[9,13–25] It is thus desirable to be able of controlling both energy level alignment and magnetic interaction. The former can be tuned by choosing the molecular species having convenient functional groups. Tailoring magnetic interactions is more difficult. Several authors have modified the interfacial exchange interaction between a ferromagnetic electrode and organic molecules by the

M. Blanco-Rey
Departamento de Polímeros y Materiales Avanzados: Física, Química y Tecnología
Universidad del País Vasco UPV/EHU
San Sebastián 20018, Spain
E-mail: maria.blanco@ehu.eus

M. Blanco-Rey, R. Castrillo, K. Ali, M. Ilyn, J. E. Ortega, F. Schiller, L. Fernández
Centro de Física de Materiales CSIC-UPV/EHU-Materials Physics Center
San Sebastián 20018, Spain
E-mail: li.fernandez@nanogune.eu

M. Blanco-Rey, R. Castrillo, K. Ali, J. E. Ortega
Donostia International Physics Center
Donostia-San Sebastián 20018, Spain

K. Ali
Chalmers University of Technology, Göteborg
Göteborg 412 96, Sweden

P. Gargiani
ALBA Synchrotron Light Source
Cerdanyola del Vallès 08290, Spain

M. Gastaldo, M. Paradinas, M. A. Valbuena, A. Mugarza
Catalan Institute of Nanoscience and Nanotechnology (ICN2)
CSIC and BIST, Campus UAB, Barcelona 08193, Spain

M. Gastaldo
J. Heyrovský Institute of Physical Chemistry
Czech Academy of Sciences
Prague 18223, Czech Republic

M. Paradinas
Institut de Ciència de Materials de Barcelona
ICMAB-CSIC, Campus UAB, Bellaterra 08193, Spain

incorporation of spacers like graphene, oxygen atoms or a Cu layer in systems formed by phtalocyanine or porphyrin molecules adsorbed on ferromagnetic Ni or Co surfaces.[11,26–28] Thus, the natural ferromagnetic (FM) interfacial exchange interaction has been turned into an antiferromagnetic (AFM) one, which is a relevant feature in the design of molecular spintronic devices.[4] Another strategy to get an interfacial AFM exchange coupling is to use $3d$ transition metal surfaces and RE-centered metal–organic molecules.[29–31]

In this work, we explore an alternative way of achieving an interfacial AFM exchange interaction by combining a ferromagnetic single-atom thick layer that incorporates RE atoms with a single monolayer of organic molecules that include transition metal atoms. For this purpose, we adsorb copper phthalocyanine (CuPc) molecules on ferromagnetic GdAu$_2$ and HoAu$_2$ single atomic layers.[32–36] A spontaneous antiparallel alignment between the CuPc spin and the magnetization of the REAu$_2$ surfaces is detected, which is induced by a superexchange interaction between the unpaired $3d$ electron of CuPc and the $4f$ electrons of the RE. Such interfacial AFM coupling has been already observed in different systems like Co nanodots grown on GdAu$_2$ MLs[37–40] or RE adatoms on Fe islands.[41] Campbell proposed a model[42] to explain the $4f$–$3d$ exchange found in RE-transition metal compounds, extensively studied in the past. This model features an intra-atomic f-sd FM exchange interaction between the RE $4f$ and the RE $6s5d$ orbitals and a subsequent interaction between the itinerant electrons of the RE and the transition metal, which can be AFM or FM depending on the exchange coupling mechanism. Furthermore, we have observed in our system that the presence of $4f$ electrons with an unquenched quantum orbital momentum L, as it is the case of Ho, introduces strong spin-orbit effects that lead to an anisotropic exchange mechanism. This unconventional feature is of interest for the development of interfaces with improved functionalities, such as an anisotropic magnetoresistance behavior.[43]

Both substrate formed by GdAu$_2$ and HoAu$_2$ monolayers (MLs) exhibit a RKKY exchange coupling between the RE atoms[34,36] and a similar Curie temperature of T_C = 19 and 22 K, respectively. However, these materials differ in their magnetic anisotropic behavior, which is defined by the RE atom. HoAu$_2$ has an out-of-plane (OOP) easy-axis of magnetization, while GdAu$_2$ has an in-plane (IP) one.[34,35,38] In the case of HoAu$_2$ the main anisotropy contribution arises from localized $4f$ electrons. On the contrary, in the case of GdAu$_2$, as Gd has an L = 0, the

magnetocrystalline anisotropy originates from specific spin-orbit splittings that take place in the RE(d)-Au(s) hybrid bands of the GdAu$_2$ band structure.[36] In this work, we explore the magnetic anisotropy of the spinterfaces formed by the adsorption of CuPc on HoAu$_2$ and GdAu$_2$ MLs, finding that the inherent OOP anisotropy of the CuPc molecule is enhanced upon adsorption on the HoAu$_2$ substrate, while it is attenuated on GdAu$_2$.

In order to characterize comprehensively our hybrid interfaces and the effect of the Gd and Ho atoms on their magnetic properties, we resort to X-ray absorption spectroscopy (XAS), X-ray magnetic circular dichroism (XMCD) and multiplet simulations. The CuPc/REAu$_2$ systems emerge as excellent candidates for this investigation, due to the weak chemical interaction of CuPc with the mentioned substrates GdAu$_2$ and HoAu$_2$.[44] Hence, we can discard strong hybridization effects and new spin-polarized interfacial states as the source for the observed robust and anisotropic AFM exchange coupling.
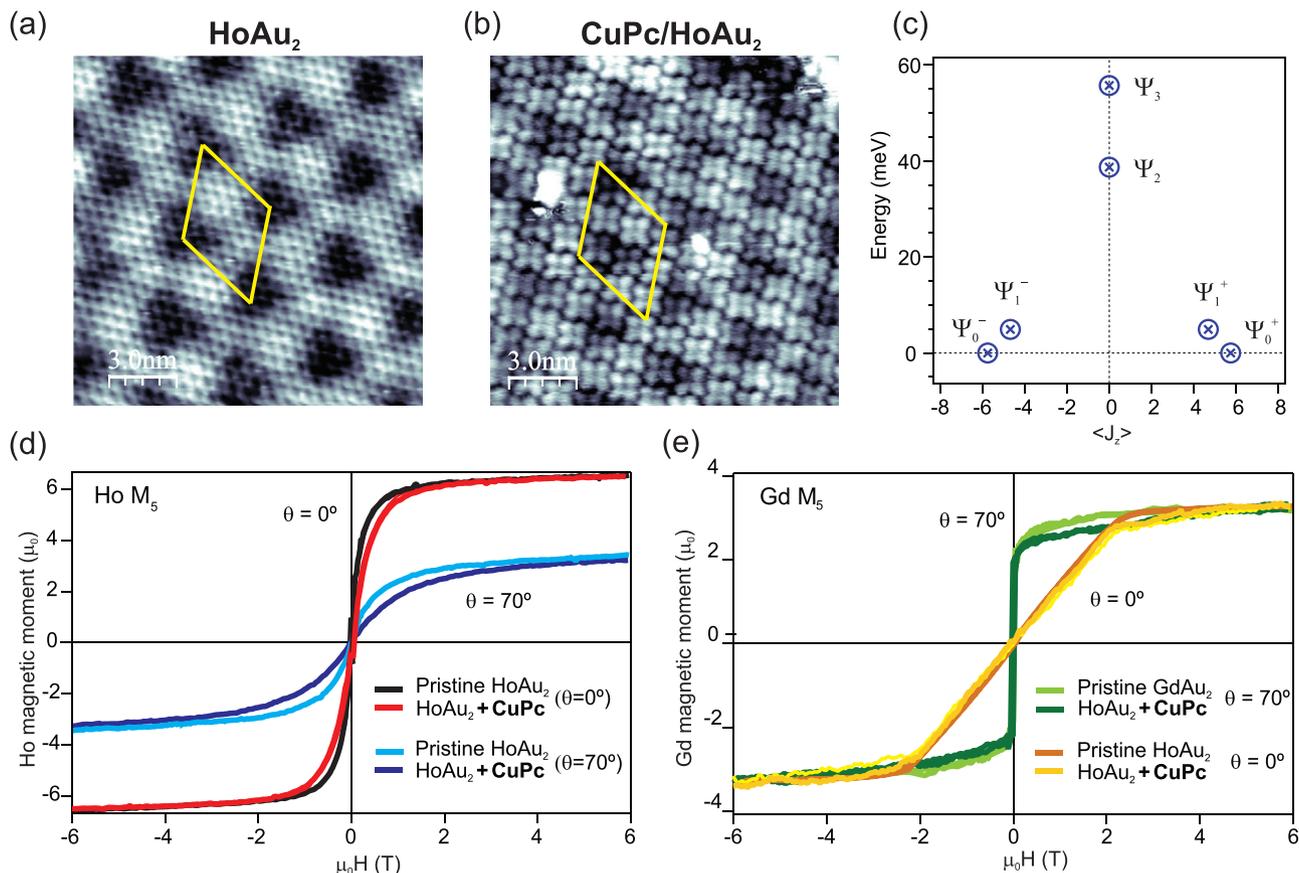
2. Results and Discussion

Monolayers (MLs) of HoAu$_2$ and GdAu$_2$ are used as substrates for the adsorption of CuPc molecules. **Figure 1a,b** displays STM images of the pristine HoAu$_2$ surface and the same covered by 1ML of CuPc. The latter is characterized by a flat and commensurated growth on top of the REAu$_2$ surface compounds.[44] Moreover, upon CuPc adsorption the representative Moiré lattice of the REAu$_2$ surfaces, formed by the lattice mismatch between Au(111) and REAu$_2$ layers is still visible. We investigate the magnetic properties of the formed hybrid metal–organic interfaces CuPc/REAu$_2$ (RE = Gd, Ho) by XAS and XMCD. With that in mind, 0.7 ML of CuPc was grown on top of both surface compounds. Spectra were recorded with circularly polarized light at the Cu L$_{2,3}$ and RE M$_{4,5}$ absorption edges in both out-of-plane (OOP) and in-plane (IP) geometries. In OOP, both the magnetic field and X-rays are perpendicular (θ = 0°) to the surface, while in IP the magnetic field and the X-rays are nearly parallel (θ = 70°) to the surface. Additionally, X-ray linear dichroism (XLD) measurements were carried out on the adsorbed CuPc to investigate its orientation with respect to the plane of the substrate (see Experimental Section).

2.1. Magnetic Robustness of REAu$_2$ Monolayers Upon CuPc Adsorption

GdAu$_2$ and HoAu$_2$ MLs display IP and OOP magnetic anisotropy, respectively, as determined by XMCD measurements.[35,36] The IP anisotropy of GdAu$_2$ arises from a band anisotropy, extensively explored by DFT calculations.[36] In contrast, HoAu$_2$ displays an OOP anisotropy that results from the $^5H_8$ configuration of the Ho $4f$ orbital, as previously determined.[35] Before turning our attention to the effect of the molecular layer, we delve further into the HoAu$_2$ anisotropy by performing multiplet simulations of the experimental XMCD spectra. The fundamental model that we use in this work to account for the magnetic properties of the HoAu$_2$ substrate is the single-ion Hamiltonian[45]

$$\mathcal{H} = \mathcal{H}_{Coulomb} + \lambda \mathbf{L} \cdot \mathbf{S} + \mu_B(\mathbf{L} + 2\mathbf{S}) \cdot \mu_0\mathbf{H} + \mathcal{H}_{CF} \tag{1}$$

M. A. Valbuena
Instituto Madrileño de Estudios Avanzados
IMDEA Nanociencia
Madrid 28049, Spain

A. Mugarza
ICREA-Institució Catalana de Recerca i Estudis Avançats
Barcelona 08010, Spain

J. E. Ortega
Departamento de Física Aplicada I
Universidad del País Vasco UPV/EHU
San Sebastián 20018, Spain

L. Fernández
CIC nanoGUNE-BRTA
San Sebastián 20018, Spain

**ADVANCED
SCIENCE NEWS**

www.advancedsciencenews.com

NANO · MICRO

small

www.small-journal.com

Figure 1. STM images at room temperature of a) $HoAu_2$ ($I = 0.3$ nA; $U = 0.7$ V) and b) 1 ML $CuPc/HoAu_2$ ($I = 0.2$ nA; $U = 0.9$ V) revealing the atomically resolved structure of the investigated systems. The solid rhombo in yellow denotes de underlying Moiré lattice of the $REAu_2$ surface compound. Image sizes are (50×50) nm^2. c) The energy splitting of the quantum levels of the Ho^{3+} (4f) orbital in the $HoAu_2$ ML obtained from the multiplet calculations. The ground state Ψ_0 and the first excited state Ψ_1 are doublets with unquenched $\langle J_z \rangle$. d,e) XMCD magnetization curves measured at 4 K on pristine $REAu_2$ and on $CuPc/REAu_2$ surfaces, RE = Ho, Gd, respectively. The loops were measured in OOP ($\theta = 0°$) and IP geometry ($\theta = 70°$) at the Ho and Gd M_5 absorbtion edge.

that will provide us with the electronic configuration of the 4f orbital. It includes on the same footing Coulomb, spin-orbit (λ is the atomic spin-orbit constant) and Zeeman terms ($\mu_0\mathbf{H}$ is the field applied on the total magnetic moment of Ho), together with a C_{3v} symmetric crystal field (CF) term parameterized in the Wybourne convention.[46] Diagonalization of Equation (1) yields the multiplet structure (i.e., electronic many-body states) of the 4f orbital, which determines the 4f contribution of Ho to the magnetocrystalline anisotropy of $HoAu_2$. In the case of $GdAu_2$, we work with a simplified form of Equation (1). Here we can take the approximation of negligible spin-orbit coupling and crystal field acting on the 4f orbital,[36] so that the 4f spectrum is simply that of a free $J = 7/2$ multiplet split by the Zeeman term. XAS and XMCD spectra are then simulated as optical transitions between those states. The Ho CF parameters are adjusted to obtain a reasonable overall agreement between simulated and experimental XAS spectra both at $\theta = 0°$ and 70° incidences. In this work, we consider three CF parameters for the fits out of the six free parameters allowed by the C_{3v} symmetry. The methodology is described in the Experimental Section and the Sections S3 and S4 (Supporting Information), where we give details about the automatized CF fitting procedure. Figure 1c shows the lowest-lying

energy levels of the Ho $J = 8$ multiplet obtained for the resulting parameterized Hamiltonian. We find that the ground state Ψ_0 is a doublet with $\langle J_z \rangle = \pm 4.7$, with an energy difference of 4.9 meV between them. For the second excited state Ψ_2, which lies at a high energy of 38.7 meV, the $\langle J_z \rangle$ value becomes quenched by the quantum tunneling allowed by the threefold symmetry of the CF. This energy value is a measure of the strong OOP magnetic anisotropy of this system. This scenario of symmetry-protected magnetic bistability is qualitatively similar to that of Ho adatoms on Cu(111),[47] with the difference that the $\langle J_z \rangle$ quenching occurs for an energy larger by one order of magnitude in the $HoAu_2$ case, which benefits the bistability preservation. The reason for this difference in the level splittings is the intense CF felt by the Ho^{3+} ion embedded in the 2D alloy structure (see Table S2, Supporting Information).

Upon CuPc adsorption, the XMCD magnetization curves of both $REAu_2$ MLs suffer small changes that consist mainly in a slight reduction of the magnetization signal, but without significant anisotropy variations. A similar behavior has been reported for organic nanowires grown on $GdAu_2$ surfaces,[48] where a decrease of ≈ 5 K in the Curie temperature (T_C) was detected as well. The XMCD magnetization is proportional to the magnetic

**ADVANCED
SCIENCE NEWS**
www.advancedsciencenews.com

**NANO · MICRO
small**
www.small-journal.com

moment of the sample, but as it is element sensitive, this value gives the magnetic response from the measured element, i.e., from the RE atoms. Figure 1 displays the XMCD loops measured at the Gd and Ho M_5 absorption edges at IP and OOP geometries, before and after adsorption of 0.7 ML of CuPc. As we know from previous studies, CuPc molecules grown on $HoAu_2$ and $GdAu_2$ surfaces form densely packed physisorbed monolayers.[44] Therefore, we do not expect that the CuPc ML significantly alters the energy levels of the Ho^{3+} multiplet (Figure 1c) or the $J = 7/2$ multiplet of Gd^{3+}. Under this assumption, the differences observed in the $REAu_2$ XMCD loops upon CuPc physisorption can be attributed to 1) the presence of a Cu–RE magnetic exchange interaction and 2) subtle changes in the RE–RE RKKY interaction. The first effect, namely the Cu–RE exchange coupling, will be analyzed and discussed in detail in Section 2.3 using the Cu L_3 intensities measured on CuPc/$REAu_2$ interfaces. To understand the crucial role of the aforementioned RKKY exchange of point (2) we begin by modeling the experimental magnetization curves of the bare substrates without such interaction. Using the single-ion Hamiltonian eigenstates and eigenergies E_i, we have simulated these curves as the expected total magnetic moments of the Ho atoms. They are calculated at finite temperature as the thermal average:

$$\langle \vec{\mu}_{J,RE} \rangle = \frac{1}{Z} \sum_i \vec{\mu}_{J,RE} e^{-E_i/k_B T} \qquad (2)$$

where Z is the partition function (in the case of Gd, this equation is reduced to the Brillouin function for $J = 7/2$). This expression, which neglects the net ferromagnetic RE–RE interactions, does not provide agreement with the experiment, as shown in Figure S4 (Supporting Information). To include these interactions, we consider an effective magnetic field on the RE total magnetic moments $\vec{B}_{eff} = \mu_0 \vec{H} + \hat{\gamma} \cdot \langle \vec{\mu}_{J,RE} \rangle$. Here, the second term is an added self-consistent field (a Weiss-like field) that corrects the eigenergies in Equation (2) by adding the corresponding Zeeman energy. In turn, this Zeeman term modifies the shape of the magnetization curves, making them steeper (see Figure S4, Supporting Information). Importantly, the $\hat{\gamma}$ tensor is anisotropic, i.e., its components differ for magnetic moments aligned parallel or perpendicular to the surface. Section S5 (Supporting Information) shows the numerical analysis of $\hat{\gamma}$ in bare $REAu_2$ substrates.

In a previous study, we detected a non-negligible impact of the CuPc adsorption on the electronic structure of $HoAu_2$ and $GdAu_2$ MLs as a result of the so-called *push-back* effect, i.e., the Pauli repulsion between the electron clouds of the metallic surface and the molecule.[44] In fact, CuPc is physisorbed on these surfaces, but there is an energy shift of the RE(d)-Au(s) surface states of about 35 meV toward the Fermi level upon CuPc adsorption. The qualitative net effect of CuPc physisorption is a modification of the magnetization curves, which become less steep than those of the corresponding bare substrates, as observed in Figure 1d. This behavior is consistent with a reduction of the self-consistent field in both substrates, i.e., an attenuation of the RKKY coupling, that would be manifested as a reduction of the Curie temperature. We recall that RKKY coupling is mediated by itinerant electrons and, therefore, any modification of the surface electronic structure by the *push-back* effect is likely to promote a change in the Curie temperature.

2.2. CuPc Magnetic Anisotropy on REAu₂ Monolayers

X-ray linear dichroism (XLD) measured at the N K (see Section S1, Supporting Information) and Cu $L_{2,3}$ edges confirm the planar adsorption of CuPc molecules on $REAu_2$ surface alloys. **Figure 2a** discloses the Cu $L_{2,3}$ XLD measurements carried out on the CuPc/$GdAu_2$ system. Due to the high background intensity arising from the Au substrate, long-range EXAFS fluctuations are induced. Therefore, the copper transition is located on top of a sinus-like curve (see inset) that is subtracted for better visualization. The white line shows a clear linear dichroism with a much larger intensity when $\vec{E}$ is parallel to the surface plane. The main peak of the XLD pattern is assigned to the transition from the Cu $2p_{x,y}$ localized orbital into the singly occupied molecular orbital (SOMO) Cu $3d_{x2-y2}$ with spin $S = 1/2$.
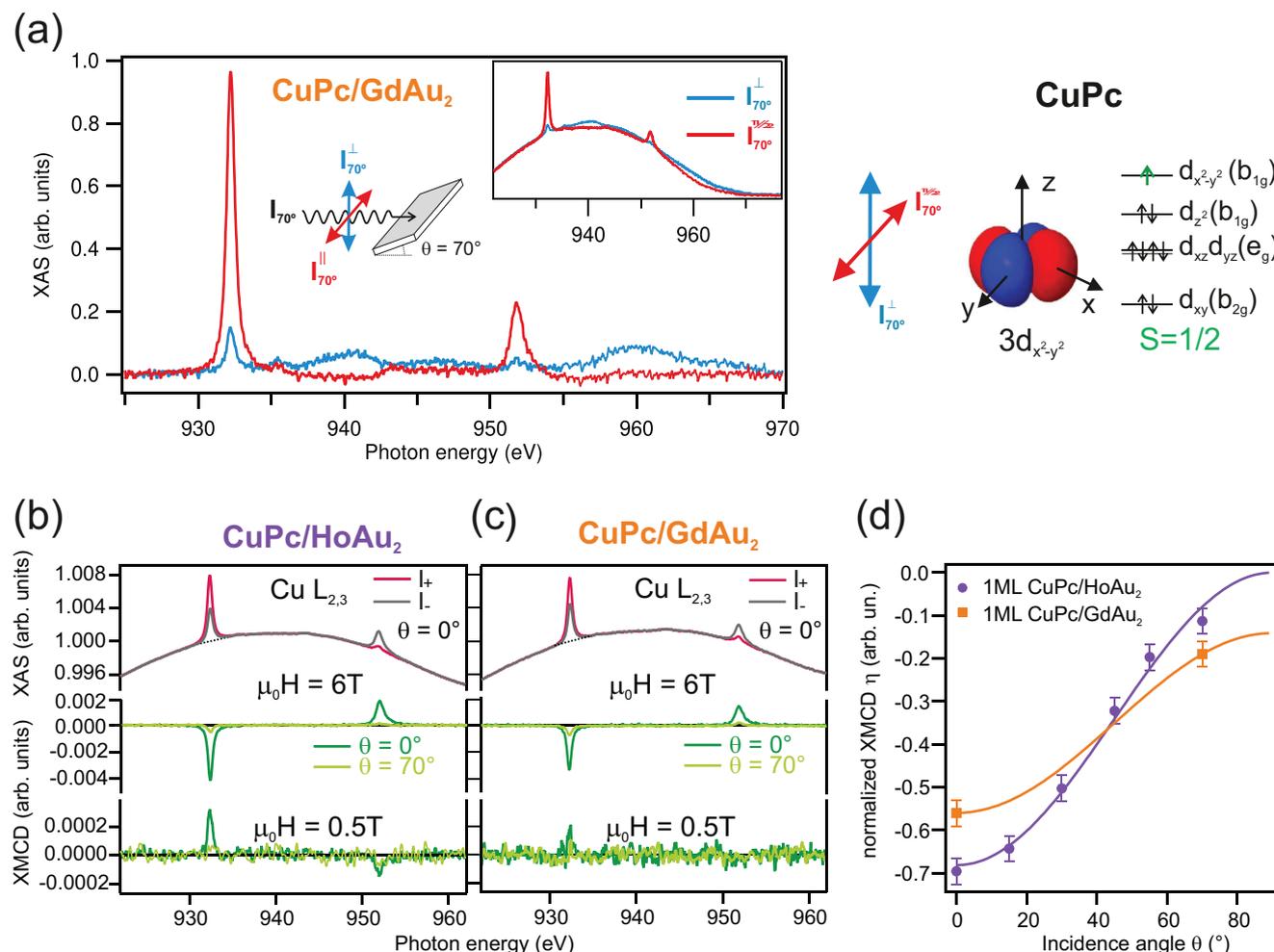
Next, we measured XAS and XMCD at the Cu $L_{2,3}$ edge at 6 and 0.5 T. Figure 2b,c shows the XAS and XMCD spectra corresponding to CuPc/$GdAu_2$ and CuPc/$HoAu_2$, respectively. An inversion in the sign of the XMCD signal at 0.5 T is detected, which indicates an antiparallel ordering of the Cu magnetic moment to the underlying $REAu_2$ substrates at low fields. The application of larger applied magnetic fields forces the Cu magnetic moment to rotate in the direction of the field due to the Zeeman effect. In order to study the magnetic anisotropy of the CuPc/$REAu_2$ interfaces, we have performed various XAS/XMCD measurements at different incidence angles of applied magnetic field/light direction. Figure 2d shows the angular dependence of the normalized L_3 XMCD intensities at 6 T. The original XAS curves were normalized by a multiplying factor such that the background at the L_3 peak has always the same intensity. The normalized XMCD intensity η is then calculated as:

$$\eta = \frac{I_+ - I_-}{\frac{I_+ + I_-}{2} - 1} \qquad (3)$$

On both substrates, the highest L_3 XMCD intensity is measured at OOP geometry ($\theta = 0°$), where the CuPc magnetization is maximum. The same behavior has been observed on CuPc MLs and submonolayers adsorbed on Ag(100) or Au(110) surfaces.[50–53] This is due to the fact that both the quantum orbital momentum L_z and the spin dipole moment T_z of CuPc show a strong OOP anisotropy.[50] In this regard, we have calculated T_z and L_z values for the bare CuPc molecule (see Section S6, Supporting Information), identifying unequivocally the intrinsic OOP anisotropy character of the free molecule. The strong L_3 intensity variation between $\theta = 0°$ and $\theta = 70°$ observed in CuPc/$HoAu_2$ is remarkable and it is shown in Figure 2d. In the CuPc/$GdAu_2$ system this variation is clearly reduced. The angular dependence of the normalized XMCD intensity can be expressed as:

$$\eta = \eta_\perp \cos^2 \theta + \eta_\parallel \sin^2 \theta \qquad (4)$$

The data points of Figure 2 allow to determine the relation $\eta_\perp \eta_\parallel$ for both systems CuPc/$HoAu_2$ and CuPc/$GdAu_2$.[51] In the case of the $HoAu_2$ substrate, this ratio results to be 11.5, while in the case of $GdAu_2$ is reduced to 4.0. Thus, it is evident that the $HoAu_2$ ML enhances the Cu L_3 signal at OOP geometry ($\theta = 0°$), and thus promotes the intrinsic OOP anisotropy of the molecule, while $GdAu_2$ attenuates it. The sum rule analysis allows to extract from

ADVANCED
SCIENCE NEWS

www.advancedsciencenews.com

NANO · MICRO

small

www.small-journal.com

Figure 2. XLD, XAS, and XMCD spectra measured at the Cu $L_{2,3}$ edge on CuPc/REAu$_2$ samples. a) XLD spectra of 1 ML CuPc on GdAu$_2$ at room temperature. Spectra were recorded with both, vertical (in red) and horizontal (in blue) polarized light at a fixed incident angle of 70°. The diagram shows the electron filling scheme for CuPc electrons. b,c) XAS and XMCD of 0.7 ML CuPc on HoAu$_2$ and GdAu$_2$, respectively measured at 4 K. The top panels indicate the XAS measurements at an applied field of 6 T in OOP geometry (normalized to 1 at the base of the L_3 peak). The lower panels (in green) reveal the XMCD spectra resulting from the XAS at IP and OOP geometry. XMCD measurements are displayed for applied fields of 6 and 0.5 T. d) Angular variation of the Cu L_3 normalized XMCD spectra η at 6 T for 1 ML CuPc/HoAu$_2$ and CuPc/GdAu$_2$. The lines follow the Equation (4) in both systems. In the case of CuPc/HoAu$_2$, it represents a fit of the data points.

the XMCD data measured at 6 T the μ_L and μ_S^{eff} values at OOP ($\theta = 0°$) and IP geometry ($\theta = 70°$). **Table 1** summarizes those values and their respective ratios in comparison with the theoretical ones for bare CuPc. The resulting ratios $\mu_L(0°)/\mu_L(70°)$ and $\mu_S^{eff}(0°)/\mu_S^{eff}(70°)$ confirm the strong OOP anisotropy of the CuPc/HoAu$_2$ system, and the importance of the match between anisotropy axes of substrate and molecule in order to get a more efficient magnetization of the molecular layer.

2.3. Anisotropic Exchange between CuPc and REAu$_2$ Substrates

The XMCD magnetization curves measured at the Cu L_3 edge of the CuPc/REAu$_2$ samples are shown in **Figure 3**. These measurements probe the Cu magnetic moment M_{Cu}. Both systems display a similar trend, but with particular features that depend on the substrate and the direction of the applied magnetic field.

At OOP geometry and low fields (below 1 T) the already observed AFM coupling between Cu and RE atoms is confirmed. It is worth to note that, in the case of the CuPc/GdAu$_2$ interface, M_{Cu} is slightly reduced compared to CuPc/HoAu$_2$. The former is related to the magnetization of the GdAu$_2$ surface, which in OOP geometry has a reduced magnetization at low fields, as it is seen in the XMCD loops of Figure 1e. The XMCD magnetization curves measured in IP geometry reveal that between 0 and 2 T M_{Cu} is zero or smaller than the experimental error in both systems. This behavior points out the relatively strong perpendicular anisotropy of CuPc, which hinders the polarization of M_{Cu} in the IP direction on both substrates. Nevertheless, at higher applied fields there is a change in the magnetization behavior due to the Zeeman interaction that induces the gradual rotation of M_{Cu} and allows a larger projection of M_{Cu} along the applied field direction and REAu$_2$ magnetization, although not reaching full saturation in either IP or OOP directions.

ADVANCED
SCIENCE NEWS
www.advancedsciencenews.com

NANO · MICRO
small
www.small-journal.com

Table 1. Magnetic moments μ_L and μ_S^{eff} of CuPc/HoAu$_2$ and CuPc/GdAu$_2$ and the magnetic moment ratios between the OOP ($\theta = 0°$) and the IP geometry ($\theta = 70°$). The values are obtained from the sum rules analysis of the XMCD measurements performed at 6 T. The error range is 0.01μ_B for μ_L (0°) and μ_L (70°). For μ_S^{eff}(0°) the error range amounts to 0.1 μ_B and for μ_S^{eff}(70°) to 0.06 μ_B. The values taken from ref. [50] were measured at 6 K and 5 T. The last row corresponds to the simulated bare CuPc values (see Section S6, Supporting Information).

	μ_L (0°) [μ_B]	μ_S^{eff} (0°) [μ_B]	μ_L (70°) [μ_B]	μ_S^{eff} (70°) [μ_B]	μ_L (0°)/μ_L (70°)	μ_S^{eff} (0°)/μ_S^{eff} (70°)
CuPc/HoAu$_2$	0.1 ± 0.01	1.35 ± 0.07	0.04 ± 0.01	0.16 ± 0.4	2.5	8.1
CuPc/GdAu$_2$	0.07 ± 0.01	1.04 ± 0.1	0.06 ± 0.01	0.27 ± 0.06	1.2	3.9
CuPc/Ag(100)[50]	0.10	1.67	0.03	0.31	3.3	5.4
CuPc (theory)	0.08	2.34	0.03	0.31	2.8	7.6

We have modeled the CuPc magnetization curves on both REAu$_2$ substrates neglecting the molecule–molecule magnetic interactions. The huge anisotropy of the spin dipole moment T_z and effective spin moment μ_S^{eff} of CuPc is reflected in a strong attenuation of the XMCD L_3 peak intensity at IP geometry. By treating Cu^{2+} as a $S = 1/2$ Zeeman-split two level system, we obtain the expectation value:

$$\langle \mu_{S,z}^{eff} \rangle (\mu_0 H) = \frac{1}{2} \tanh \frac{\mu_{S,z}^{eff}(\mu_0 H + \mathcal{J}_{ex}\langle \mu_{J,RE,z}^{eff} \rangle)}{k_B T} \quad (5)$$

Here, the quantities to be adjusted are $\mathcal{J}_{ex}$, which represents the magnetic exchange between the Cu and RE atoms, and $\mu_{S,z}^{eff}$,

which is the Cu saturated effective spin moment projection on the applied field ($\mu_0 H$) direction. The substrate magnetization as a function of the applied field $\mu_0 H$ enters in the model as the calculated RE expected effective total moment projections $\langle \mu_{J,RE,z}^{eff} \rangle$, shown in Figure S5 (Supporting Information). This way, the model accounts for the anisotropic features of HoAu$_2$ and GdAu$_2$ surfaces. The experimental data fits this model and the resulting $\mathcal{J}_{ex}$ values are included in Figure 3 as solid lines for OOP and IP geometry (see additional details in the S8, Supporting Information). The intensities have been normalized to the μ_S^{eff} values extracted from the sum rules values of Table 1. The field at which $\langle \mu_{S,z}^{eff} \rangle$ cancels out is proportional to the AFM exchange coupling constants $\mathcal{J}_{ex}$ between Cu and RE atoms. The low orders of
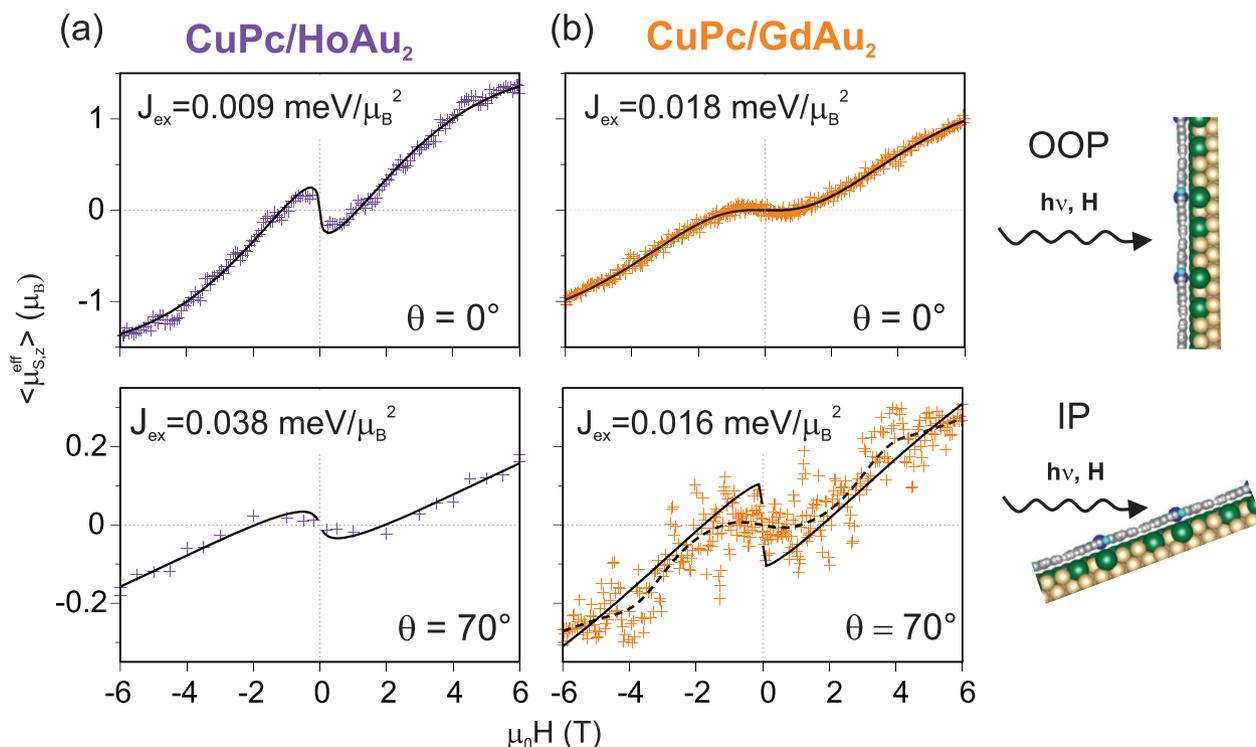
Figure 3. XMCD magnetization curves and simulations at the Cu L$_3$ edge of a) CuPc/HoAu$_2$, and b) CuPc/HoAu$_2$ hybrid interfaces. The experimental data measured at 4 K in OOP ($\theta = 0°$) and IP ($\theta = 70°$) geometries are represented in purple (orange) for CuPc/HoAu$_2$ (CuPc/GdAu$_2$). The solid black lines display the theoretical model. In the bottom-right panel, the dashed line is a smoothed representation of the scattered experimental data to guide the eye. To compare the data, the experimental intensities are normalized to the experimental $\langle \mu_{S,z}^{eff} \rangle$ values obtained by sum rules analysis at 6 T (see Table 1). The labels $\mathcal{J}_{ex}$ indicate the Cu–Ho and Cu–Gd exchange coupling constants obtained from fits to Equation (5).

ADVANCED
SCIENCE NEWS

www.advancedsciencenews.com

NANO · MICRO
small
www.small-journal.com

magnitude of the fitted $\mathcal{J}_{ex}$ (≈ 0.01 meV per μ_B^2) are consistent with the weak physisorption of CuPc on REAu$_2$[44] and similar to those reported in the literature for TbPc$_2$ on Ni substrates.[29] The fits show a pronounced anisotropic behavior of the Cu–Ho exchange. The ratio between the exchange constants for IP and OOP applied fields in this case is $\mathcal{J}_{ex}^{70°}/\mathcal{J}_{ex}^{0°} = 4.2$, whereas the Cu–Gd exchange is more isotropic with $\mathcal{J}_{ex}^{70°}/\mathcal{J}_{ex}^{0°} = 1.1$. Similar strongly anisotropic interactions between metal–organic molecules and ferromagnetic substrates have also been reported for the Cu4Dint molecule (a Cu-tetraazaporphyrin with substituents) on Fe$_3$O$_2$[54] and TbPc$_2$ on oxidized and reduced Ni thin films.[29] In these systems, the coupling follows a superexchange mechanism, where the organic ligands play a determinant role as intermediate orbitals for hopping.[55–57] These superexchange interactions show anisotropy as a consequence of spin-orbit coupling.[58–60] In the Cu4Dint case the IP and OOP $\mathcal{J}_{ex}$ have similar magnitudes and different signs, i.e., the antiferromagnetic coupling can be switched to ferromagnetic by grazing to the normal rotation of the applied field. This dramatic effect is explained by the dominance of the Fe–O–Cu and Fe–N–Cu superexchange paths, respectively. In the TbPc$_2$ case the exchange anisotropy is modulated by the evaporation of O and Li on the Ni surface, which induces Ni quantum orbital moment changes (albeit the doped films continue to show perpendicular anisotropy), with IP-to-OOP $\mathcal{J}_{ex}$ ratios ranging between 1.5 and 0.3, approximately. In our systems, we have achieved a wider ratio by using in the substrate composition REs of the lowest and largest possible orbital magnetic moments, namely $L = 0$ for Gd and $L = 6$ for Ho. Anisotropic exchange interactions are enhanced by the presence of states with orbital degeneracies, a mechanism known as orbital-dependent exchange (ODE).[59–65] This mechanism is relevant in the case of $3d - 3d$ and $4f - 3d$ exchange interactions in crystals and molecular magnets.[66,67] In particular, in systems where the RE orbital moment L is unquenched, ODE is enhanced.[63,68–70] Indeed, the analysis of Figure 3 shows that the ODE effect is smaller for CuPc on GdAu$_2$ ($L = 0$) than on HoAu$_2$ ($L = 6$).

3. Conclusion

We have confirmed the AFM coupling established at the hybrid metal–organic interface between a CuPc monolayer and a ferromagnetic single atomic layer of REAu$_2$ (RE = Gd, Ho). The latter is set by a $3d$–$4f$ superexchange interaction between Cu and RE atoms. Moreover, this AFM coupling across the interface seems to be robust up to ≈ 1.5 T. The natural OOP anisotropy of a CuPc ML is promoted upon adsorption on the HoAu$_2$ substrate, which shows an OOP easy axis of magnetic anisotropy. It is worth noting that CuPc molecules are physisorbed on REAu$_2$ surfaces and do not display strong hybridization or chemical interaction with the substrate. In this context, the aforementioned magnetic properties cannot be ascribed to the generation of a new spin-polarized interfacial state, as is often the case in strongly hybridized spinterfaces. The use of RE atoms introduces strong spin-orbit effects that may promote a large anisotropic exchange coupling between the Cu and RE atoms. This is the case of the hybrid spin interface CuPc/HoAu$_2$, which displays an exchange interaction that is four times stronger for magnetic fields applied in IP geometry than in the OOP one, whereas CuPc/GdAu$_2$ ex-

hibits isotropic exchange coupling. We explain this behavior by the orbital-dependent exchange mechanism, which appears in systems with an unquenched orbital moment L, this is, states with an orbital degeneracy. The effect of anisotropic exchange coupling found in the hybrid interface CuPc/HoAu$_2$ arises as a relevant result for the development of magneto-resistive devices with extended functionalities, allowing modulation of the coupling strength upon a 90° rotation of the external field. In conclusion, the stable AFM coupling at the metal–organic interfaces of CuPc/REAu$_2$ can show a tunable anisotropic character, depending on the RE atom of the substrate, which represents a step forward in the field of molecular spintronics.

4. Experimental Section

Samples were prepared in an ultra-high vacuum (UHV) chamber at a base pressure of 2×10^{-10} mbar. Several Au(111) single crystals were used as substrates, that were cleaned by cycles of Ar$^+$ ion sputtering ($E_{kin} = 1$ keV) and annealing to 500°C. The different RE-Au$_2$ surface compounds were grown in situ by evaporation of small amounts of RE atoms on the Au(111) surface, held at a fixed temperature. The optimal growth temperature for the substrate was 420°C for HoAu$_2$ and varies between 400 and 450°C for GdAu$_2$. Below these temperatures, the characteristic Moiré was not well formed, and above them, the RE metals start to diffuse into the bulk or re-evaporate from the surface. The evaporation rate of the RE atoms was 0.03 ML min^{-1}. CuPc molecules were evaporated on the REAu$_2$ surface with deposition rates of 0.05 ML min^{-1}. The pressure in the chamber during evaporation was of 8×10^{-10} mbar. The calibration of the CuPc layer thickness was carried out by gradual depositions of CuPc/Au(111) and the subsequent low energy electron diffraction (LEED) analysis. The coverage of the first visible diffraction spots of the molecules at RT was defined as 0.9 ML.[71] The substrate temperature during CuPc evaporation was set to room temperature.

XMCD and XLD experiments were realized at the BOREAS beamline of the ALBA synchrotron radiation facility in Spain. Absorption spectra were acquired in total electron yield at the Cu L$_{2,3}$ as well as Ho and Gd M$_{4,5}$ edges. XLD spectra were collected at room temperature at an incidence angle of 70°, rotating the light polarization from vertical ($\vec{E}$ in plane) to horizontal ($\vec{E}$ out of plane). XMCD spectra were acquired at different photon and magnetic field incidence angles (from $\theta = 0°$ to $\theta = 70°$) in order to study the magnetic anisotropy of the different interfaces. Error bars of the orbital and angular moments (see Table 1) were calculated by varying the Cu L$_3$ and L$_2$ edge integration limits a few eV to maximize/minimize the integrals due to the statistical noise in the XAS and XMCD data. In out-of-plane (OOP) geometry the light propagation vector and the applied magnetic field were normal to the sample surface, while in in-plane (IP) geometry the magnetic field was nearly parallel to the surface. For the case of CuPc, 99% of circularly polarized light was used at the Cu L$_{2,3}$ edge, while rare-earth edges were acquired with 90% polarization. XMCD measurements were carried out at or below 4 K with a variable magnetic field up to ± 6 T. The XMCD spectrum was the difference between the two X-ray absorption spectroscopy (XAS) spectra recorded with the opposite orientation of the magnetic field and/or the circular helicity of the light, which were called I_+ and I_- for simplicity. The XMCD signal was proportional to the projection of the magnetization in the direction of the applied magnetic field. Element-sensitive magnetization loops were measured by sweeping the photon energies corresponding to the maximum of the XMCD asymmetry signal at the Cu L$_3$, Ho and Gd M$_5$ absorption edges and a pre-edge energy as a function of the magnetic field. The latter was used for normalization and accounts for possible instabilities of the light entering the experimental station. Further details are given in the Section S9. Sum rules were used to obtain orbital μ_L and effective spin μ_S^{eff} moments of CuPc at $\mu_0 H = 6$ T.[72,73] The effective spin moment μ_S^{eff} refers to the measurable value of the expectation values of total atomic spin (S) and spin dipole T_z

operators with $\mu_S^{eff} = 2S + 7T_z$. Both orbital and effective dipole momenta depend on the number of electron holes n in the d and f shell. For the elements considered here Cu, Ho, and Gd, the electron holes were set as $n = 1$ in the Cu d-shell and $n = 4$ and 7 for Ho and Gd holes in the f-shell, respectively. The sum $\mu_L + \mu_S^{eff}$ was used to normalize the XMCD magnetization curves.

Theoretical Model: For a given $4f^n$ occupancy of the Ho ion the XAS and XMCD $M_{4,5}$ absorption edges spectra of the bare HoAu$_2$ substrate were simulated with the code Xclaim[46] by considering electronic transitions $3d \rightarrow 4f$ in a model Hamiltonian for the $4f$ orbital, where hybridization of $4f$ electrons was neglected. In this work, the crystal field parameters were optimized to match the simulated and experimental lineshapes of the I_+, I_- measured intensities at normal and grazing (70° off-normal) incidences. Four data sets were simultaneously fit in an automated procedure, which is described in the Section S3 (Supporting Information) along with further details of the Hamiltonian parameterization. From the Hamiltonian eigenergies and eigenstates the expectation values $\langle J_z \rangle$ of the Ho^{3+} total magnetic moment projection on the field direction were calculated, which provide a model of the HoAu$_2$ magnetization curves. Similarly, using suitable crystal field parameters,[74] a single ion Hamiltonian for Cu^{2+} in CuPc was written and diagonalized (see Section S6, Supporting Information).

Supporting Information

Supporting Information is available from the Wiley Online Library or from the author.

Acknowledgements

Conflict of Interest

The authors declare no conflict of interest.

Data Availability Statement

The data that support the findings of this study are available from the corresponding author upon reasonable request.

Keywords

[1] S. Heutz, C. Mitra, W. Wu, A. Fisher, A. Kerridge, M. Stoneham, T. H. Harker, J. Gardener, H.-H. Tseng, T. S. Jones, C. Renner, G. Aeppli, *Adv. Mater.* **2007**, *19*, 3618.

[2] T. Moorsom, M. Wheeler, T. Mohd Khan, F. Al Ma'Mari, C. Kinane, S. Langridge, D. Ciudad, A. Bedoya-Pinto, L. Hueso, G. Teobaldi, V. K. Lazarov, D. Gilks, G. Burnell, B. J. Hickey, O. Cespedes, *Phys. Rev. B* **2014**, *90*, 125311.

[3] L. Margheriti, D. Chiappe, M. Mannini, P. Car, P. Sainctavit, M.-A. Arrio, F. B. de Mongeot, J. C. Cezar, F. M. Piras, A. Magnani, E. Otero, A. Caneschi, R. Sessoli, *Adv. Mater.* **2010**, *22*, 5488.

[4] H.-J. Jang, C. A. Richter, *Adv. Mater.* **2017**, *29*, 1602739.

[5] A. Cornia, P. Seneor, *Nat. Mater.* **2017**, *16*, 505.

[6] M. Cinchetti, V. A. Dediu, L. E. Hueso, *Nat. Mater.* **2017**, *16*, 507.

[7] M. J. Comstock, N. Levy, A. Kirakosian, J. Cho, F. Lauterwasser, J. H. Harvey, D. A. Strubbe, J. M. J. Fréchet, D. Trauner, S. G. Louie, M. F. Crommie, *Phys. Rev. Lett.* **2007**, *99*, 038301.

[8] J. Brede, N. Atodiresei, S. Kuck, P. Lazić, V. Caciuc, Y. Morikawa, G. Hoffmann, S. Blügel, R. Wiesendanger, *Phys. Rev. Lett.* **2010**, *105*, 047204.

[9] T. D. Nguyen, E. Ehrenfreund, Z. V. Vardeny, *Science* **2012**, *337*, 204.

[10] V. A. Dediu, *Nat. Phys.* **2013**, *9*, 210.

[11] M. Gruber, F. Ibrahim, S. Boukari, L. Joly, V. Da Costa, M. Studniarek, M. Peter, H. Isshiki, H. Jabbar, V. Davesne, J. Arabski, E. Otero, F. Choueikani, K. Chen, P. Ohresser, W. Wulfhekel, F. Scheurer, E. Beaurepaire, M. Alouani, W. Weber, M. Bowen, *Nano Lett.* **2015**, *15*, 7921.

[12] X. Sun, S. Vélez, A. Atxabal, A. Bedoya-Pinto, S. Parui, X. Zhu, R. Llopis, F. Casanova, L. E. Hueso, *Science* **2017**, *357*, 677.

[13] Z. H. Xiong, D. Wu, J. Valy Vardeny, Shi, *Nature* **2004**, *427*, 821.

[14] C. Barraud, P. Seneor, R. Mattana, S. Fusil, K. Bouzehouane, C. Deranlot, P. Graziosi, L. Hueso, I. Bergenti, V. Dediu, F. Petroff, A. Fert, *Nat. Phys.* **2010**, *6*, 615.

[15] S. Sanvito, *Nat. Phys.* **2010**, *6*, 210.

[16] S. Javaid, M. Bowen, S. Boukari, L. Joly, J.-B. Beaufrand, X. Chen, Y. J. Dappe, F. Scheurer, J.-P. Kappler, J. Arabski, W. Wulfhekel, M. Alouani, E. Beaurepaire, *Phys. Rev. Lett.* **2010**, *105*, 077201.

[17] M. Urdampilleta, S. Klyatskaya, J.-P. Cleuziou, M. Ruben, W. Wernsdorfer, *Nat. Mater.* **2011**, *10*, 502.

[18] S. Lach, A. Altenhof, K. Tarafder, F. Schmitt, M. E. Ali, M. Vogel, J. Sauther, P. M. Oppeneer, C. Ziegler, *Adv. Funct. Mater.* **2012**, *22*, 989.

[19] F. Djeghloul, F. Ibrahim, M. Cantoni, M. Bowen, L. Joly, S. Boukari, P. Ohresser, F. Bertran, P. L. Fe'vre, P. Thakur, F. Scheurer, T. Miyamachi, R. Mattana, P. Seneor, A. Jaafar, C. Rinaldi, S. Javaid, J. Arabski, J. P. Kappler, W. Wulfhekel, N. B. Brookes, R. Bertacco, A. Taleb-Ibrahimi, M. Alouani, E. Beaurepaire, W. Weber, *Sci. Rep.* **2013**, *3*, 1272.

[20] F. Al Ma'Mari, T. Moorsom, G. Teobaldi, W. Deacon, T. Prokscha, H. Luetkens, S. Lee, G. E. Sterbinsky, D. A. Arena, D. A. MacLaren, M. Flokstra, M. Ali, M. C. Wheeler, B. Gavin Burnell, *Nature* **2015**, *524*, 69.

[21] C. Wäckerlin, F. Donati, A. Singha, R. Baltic, A. Uldry, B. Delley, S. Rusponi, J. Dreiser, *Chem. Commun.* **2015**, *51*, 12958.

[22] A. Droghetti, P. Thielen, I. Rungger, N. Haag, N. Großmann, J. Stöckl, B. Stadtmüller, M. Aeschlimann, S. Sanvito, M. Cinchetti, *Nat. Commun.* **2016**, *7*, 12668.

[23] W. Si, J. Li, G. Li, C. Jia, X. Guo, *J. Mater. Chem. C* **2024**, *12*, 751.

[24] T. Bathon, P. Sessi, K. A. Kokh, O. E. Tereshchenko, M. Bode, *Nano Lett.* **2015**, *15*, 2442.

[25] S. Boukari, H. Jabbar, F. Schleicher, M. Gruber, G. Avedissian, J. Arabski, V. Da Costa, G. Schmerber, P. Rengasamy, B. Vileno, W. Weber, M. Bowen, E. Beaurepaire, *Nano Lett.* **2018**, *18*, 4659.

[26] G. Avvisati, C. Cardoso, D. Varsano, A. Ferretti, P. Gargiani, M. G. Betti, *Nano Lett.* **2018**, *18*, 2268.

[27] M. Bernien, J. Miguel, C. Weis, M. E. Ali, J. Kurde, B. Krumme, P. M. Panchmatia, B. Sanyal, M. Piantek, P. Srivastava, K. Baberschke, P. M. Oppeneer, O. Eriksson, W. Kuch, H. Wende, *Phys. Rev. Lett.* **2009**, *102*, 047202.

[28] A. Halder, S. Bhandary, D. D. O'Regan, S. Sanvito, A. Droghetti, *Phys. Rev. Mater.* **2023**, *7*, 064409.

[29] A. Lodi Rizzini, C. Krull, T. Balashov, J. J. Kavich, A. Mugarza, P. S. Miedema, P. K. Thakur, V. Sessi, S. Klyatskaya, M. Ruben, S. Stepanow, P. Gambardella, *Phys. Rev. Lett.* **2011**, *107*, 177205.

[30] A. Lodi Rizzini, C. Krull, A. Mugarza, T. Balashov, C. Nistor, R. Piquerel, S. Klyatskaya, M. Ruben, P. M. Sheverdyaeva, P. Moras, C. Carbone, C. Stamm, P. S. Miedema, P. K. Thakur, V. Sessi, M. Soares, F. Yakhou-Harris, J. C. Cezar, S. Stepanow, P. Gambardella, *Surf. Sci.* **2014**, *630*, 361.

[31] D. Klar, S. Klyatskaya, A. Candini, B. Krumme, K. Kummer, P. Ohresser, V. Corradini, V. de Renzi, R. Biagi, L. Joly, J. Kappler, U. del Pennino, M. Affronte, H. Wende, M. Ruben, *Beilstein J. Nanotechnol.* **2013**, *4*, 320.

[32] M. Ormaza, L. Fernández, S. Lafuente, M. Corso, F. Schiller, B. Xu, M. Diakhate, M. J. Verstraete, J. E. Ortega, *Phys. Rev. B* **2013**, *88*, 125405.

[33] M. Corso, M. J. Verstraete, F. Schiller, M. Ormaza, L. Fernández, T. Greber, M. Torrent, A. Rubio, J. E. Ortega, *Phys. Rev. Lett.* **2010**, *105*, 016101.

[34] M. Ormaza, L. Fernández, M. Ilyn, A. Magaña, B. Xu, M. J. Verstraete, M. Gastaldo, M. A. Valbuena, P. Gargiani, A. Mugarza, A. Ayuela, L. Vitali, M. Blanco-Rey, F. Schiller, J. E. Ortega, *Nano Lett.* **2016**, *16*, 4230.

[35] L. Fernandez, M. Blanco-Rey, R. Castillo-Bodero, M. Ilyn, K. Ali, E. Turco, M. Corso, M. Ormaza, P. Gargiani, M. A. Valbuena, A. Mugarza, P. Moras, P. M. Sheverdyaeva, A. K. Kundu, M. Jugovac, C. Laubschat, J. E. Ortega, F. Schiller, *Nanoscale* **2020**, *12*, 22258.

[36] M. Blanco-Rey, R. Castillo-Bodero, K. Ali, P. Gargiani, F. Bertran, P. M. Sheverdyaeva, J. E. Ortega, L. Fernández, F. Schiller, *Phys. Rev. Res.* **2022**, *4*, 013237.

[37] L. Fernández, M. Blanco-Rey, M. Ilyn, L. Vitali, A. Magaña, A. Correa, P. Ohresser, J. E. Ortega, A. Ayuela, F. Schiller, *Nano Lett.* **2014**, *14*, 2977.

[38] A. Cavallin, L. Fernández, M. Ilyn, A. Magaña, M. Ormaza, M. Matena, L. Vitali, J. E. Ortega, C. Grazioli, P. Ohresser, S. Rusponi, H. Brune, F. Schiller, *Phys. Rev. B* **2014**, *90*, 235419.

[39] L. Fernández, M. Corso, F. Schiller, M. Ilyn, M. Holder, J. E. Ortega, *Appl. Phys. Lett.* **2010**, *96*, 013107.

[40] L. Fernández, M. Ilyn, A. Magaña, L. Vitali, J. Ortega, F. Schiller, *Adv. Sci.* **2016**, *14*, 1600187.

[41] D. Coffey, J. L. Diez-Ferrer, D. Serrate, M. Ciria, C. de la Fuente, J. I. Arnaudas, *Sci. Rep.* **2015**, *5*, 13709.

[42] I. A. Campbell, *J. Phys. F: Metal Phys.* **1972**, *2*, L47.

[43] C. Barraud, K. Bouzehouane, C. Deranlot, S. Fusil, H. Jabbar, J. Arabski, R. Rakshit, D.-J. Kim, C. Kieber, S. Boukari, M. Bowen, E. Beaurepaire, P. Seneor, R. Mattana, F. Petroff, *Phys. Rev. Lett.* **2015**, *114*, 206603.

[44] R. Castillo-Bodero, M. Blanco-Rey, K. Ali, J. E. Ortega, F. Schiller, L. Fernández, *Nanoscale* **2023**, *15*, 4090.

[45] F. de Groot, *Coord. Chem. Rev.* **2005**, *249*, 31.

[46] J. Fernandez-Rodriguez, B. Toby, M. van Veenendaal, *J. Electron Spectrosc. Relat. Phenom.* **2015**, *202*, 81.

[47] F. Donati, A. Singha, S. Stepanow, C. Wäckerlin, J. Dreiser, P. Gambardella, S. Rusponi, H. Brune, *Phys. Rev. Lett.* **2014**, *113*, 237201.

[48] M. Abadía, M. Ilyn, I. Piquero-Zulaica, P. Gargiani, C. Rogero, J. E. Ortega, J. Brede, *ACS Nano* **2017**, *11*, 12392.

[49] S. Carniato, Y. Luo, H. Ågren, *Phys. Rev. B* **2001**, *63*, 085105.

[50] S. Stepanow, A. Mugarza, G. Ceballos, P. Moras, J. C. Cezar, C. Carbone, P. Gambardella, *Phys. Rev. B* **2010**, *82*, 014405.

[51] P. Gargiani, G. Rossi, R. Biagi, V. Corradini, M. Pedio, S. Fortuna, A. Calzolari, S. Fabris, J. C. Cezar, *Phys. Rev. B* **2013**, *87*, 165407.

[52] J. F. F. Juan Bartolomé, F. Luis, *Molecular Magnets: Physics and Applications*, Springer-Verlag Berlin Heidelber, **2014**.

[53] A. Mugarza, R. Robles, C. Krull, R. Korytár, N. Lorente, P. Gambardella, *Phys. Rev. B* **2012**, *85*, 155437.

[54] J. Klanke, E. Rentschler, K. Medjanik, D. Kutnyakhov, G. Schönhense, S. Krasnikov, I. V. Shvets, S. Schuppler, P. Nagel, M. Merz, H. J. Elmers, *Phys. Rev. Lett.* **2013**, *110*, 137202.

[55] J. B. Goodenough, *Phys. Rev.* **1955**, *100*, 564.

[56] J. B. Goodenough, *J. Phys. Chem. Solids* **1958**, *6*, 287.

[57] J. Kanamori, *J. Phys. Chem. Solids* **1959**, *10*, 87.

[58] T. Moriya, *Phys. Rev. Lett.* **1960**, *4*, 228.

[59] T. Moriya, *Phys. Rev.* **1960**, *120*, 91.

[60] T. Oguchi, *J. Phys. Soc. Jpn.* **1965**, *20*, 2236.

[61] J. M. Baker, *Rep. Prog. Phys.* **1971**, *34*, 109.

[62] D. Dai, H. Xiang, M.-H. Whangbo, *J. Comput. Chem.* **2008**, *29*, 2187.

[63] A. Palii, B. Tsukerblat, S. Klokishner, K. R. Dunbar, J. M. Clemente-Juan, E. Coronado, *Chem. Soc. Rev.* **2011**, *40*, 3130.

[64] K. W. H. Stevens, *Rev. Mod. Phys.* **1953**, *25*, 166.

[65] Moriya's derivation[59] shows the existence of anisotropic exchange contributions in the context of an orbitally non-degenerate ground state. In non-centrosymmetric systems, there is a contribution of the first order in the SOC parameter λ, commonly regarded as the Dzyaloshinskii–Moriya interaction between canted spins $\vec{D}\vec{S}_1 \times \vec{S}_2$. A second-order symmetric contribution exists with the form $\vec{S}_1 \cdot \mathcal{J}_{ex} \cdot \vec{S}_2$, which also appears in the case of centrosymmetric systems (see also ref. [64]). Oguchi developed a similar theory[60] of anisotropic exchange for systems with orbital degeneracy ($L \neq 0$). Starting with the usual isotropic Heisenberg exchange and SOC terms, the Hamiltonian is rewritten and pseudo-orbital and pseudo-spin moments as new effective degrees of freedom, which show anisotropic exchange interactions of first order in λ.

[66] J. Liu, F. de Boer, P. de Châtel, R. Coehoorn, K. Buschow, *J. Magn. Magn. Mater.* **1994**, *132*, 159.

[67] L. Rosado Piquer, E. C. Sañudo, *Dalton Trans.* **2015**, *44*, 8771.

[68] J. Borrás-Almenar, E. Coronado, J. Clemente-Juan, A. Palii, B. Tsukerblat, *J. Solid State Chem.* **2001**, *159*, 268.

[69] A. V. Palii, B. S. Tsukerblat, J. M. Clemente-Juan, E. Coronado, *Inorg. Chem.* **2005**, *44*, 3984.

[70] J. Dreiser, K. S. Pedersen, C. Piamonteze, S. Rusponi, Z. Salman, M. E. Ali, M. Schau-Magnussen, C. A. Thuesen, S. Piligkos, H. Weihe, H. Mutka, O. Waldmann, P. Oppeneer, J. Bendix, F. Nolting, H. Brune, *Chem. Sci.* **2012**, *3*, 1024.

[71] B. Stadtmüller, I. Kröger, F. Reinert, C. Kumpf, *Phys. Rev. B* **2011**, *83*, 085416.

[72] B. T. Thole, P. Carra, F. Sette, G. van der Laan, *Phys. Rev. Lett.* **1992**, *68*, 1943.

[73] P. Carra, B. T. Thole, M. Altarelli, X. Wang, *Phys. Rev. Lett.* **1993**, *70*, 694.

[74] A. Rosa, E. J. Baerends, *Inorg. Chem.* **1994**, *33*, 584.